Multi-Contact Bilateral Telemanipulation with Kinematic Asymmetries

Gionata Salvietti, *Member, IEEE,* Leonardo Meli, *Student Member, IEEE,* Guido Gioioso, *Student Member, IEEE,*
Monica Malvezzi, *Member, IEEE,* and Domenico Prattichizzo *Fellow, IEEE*

***Abstract*—We propose a novel bilateral telemanipulation framework to tame master and slave devices having different structures. This condition applies to multi-contact teleoperation scenarios where the number of contact points on the slave side and the number of interaction points on the master side are different. An example is a master device interacting with the thumb and the index fingertips of the human operator and, as slave device, a robotic arm with a multi-fingered robotic hand. In case of a manipulation task, it is not straightforward to transmit motion commands and reflect forces from the interaction with the environment. A general telemanipulation framework, that does not consider the specific kinematics of the devices involved, is needed. The main idea of this work is to take advantage of a virtual object as a mediator between the master and slave side. The arising forward and backward mapping algorithms are able to relate the motions and the exerted forces of very dissimilar systems. The approach has been evaluated in a case study consisting of two haptic interfaces used both to track the index and thumb motions and to render forces on the master side and a robotic arm with a multi-fingered hand as end-effector on the slave side. The results presented in this paper can be extended to cooperative grasping scenarios where multiple robots tele-manipulate the same object.**

***Index Terms*—Bilateral telemanipulation, Force Rendering, Cooperative Grasping.**

I. INTRODUCTION

BILATERAL telemanipulation deals with the possibility of extending remotely human manipulation capabilities by providing the user with similar conditions to that present in the remote location [1]. This is achieved typically using two subsystems called master and slave. The former is an interface for the human user which is able to capture human commands and display back forces or other important signals measured where the task is actually executed. The latter is a robot in contact with the remote environment and physically performing the task. Many works studied stability issues due to the delay introduced by the communication media, e.g., see [2, 3, 4]. Another important deeply investigated aspect has been the transparency of the teleoperation system, e.g., see [5, 6, 7]. Most of the research efforts have been focused on architectures with a single interaction point on the master and a single contact point on the slave. However, complex teleoperation tasks, as well as emergent network-based applications, need the development of more sophisticated teleoperation architectures where master and/or slave are systems establishing multiple contacts with the operator and/or the environment [8]. In [9, 10, 11], for instance, distributed bilateral control frameworks that guarantee coordinated motion between a single master and multiple slave agents considering communication delays are presented. These works can be seen as part of a larger set of *asymmetric* teleoperation systems. Such asymmetries may involve the lack of an actuator on the master manipulator or the lack of a sensor on the slave manipulator and refer to a single-master and single-slave architecture [12, 13]. Asymmetries may also arise if different number of master and slave devices are considered [14, 15]. This last definition of asymmetries is more close to the case of telemanipulation, which is the focus of this work. In fact, master and slave devices for telemanipulation can have a dissimilar kinematic structure, which may lead to a different number of interaction points on the master side and of contact points in the slave side. We define as *interaction points* on the master side the contacts between the human hand and the devices used for providing force feedback. On the slave side, *contact points* arise between the robot end-effector (e.g., a multi-fingered hand) and the grasped object. Consider for instance the case study reported in [16]. The authors studied a flexible controller to let two master single-contact devices teleoperate three slave robots cooperatively

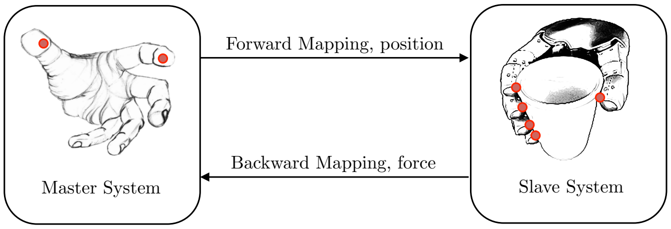

Fig. 1. General bilateral telemanipulation framework. On the master system, red dots represent the points that are tracked and the points where force is fed back to the user. On the slave side, red dots represent the contact points with the object and the points where forces are measured. The kinematics of master and slave as well as the number of contact points may differ in the considered approach.

The research leading to these results has received funding from the European Union's Horizon 2020 research and innovation programme under grant agreement n645599 of the project "SoMa" and European Union Seventh Framework Programme FP7 under grant agreement n601165 of the project "WEARHAP", and from the Italian Ministry of Education, Universities and Research Futuro in Ricerca 2012 Programme with project "MODELACT" (Code RBFR12C608).

G. Salvietti, L. Meli, G. Gioioso, M. Malvezzi and D. Prattichizzo are with the Department of Information Engineering and Mathematics, University of Siena, Siena - Italy, e-mail: [salviettigio, meli, gioioso, malvezzi, prattichizzo]@dii.unisi.it.

G. Salvietti, M. Malvezzi and D. Prattichizzo are also with the Department of Advanced Robotics, Istituto Italiano di Tecnologia, Via Morego 30, 16163 Genova, Italy.

grasping an object with one contact point per robot. The study can be generalized to consider n interaction points on the master side teleoperating m contact points on the slave side, where n can be different from m. Some solutions have been proposed in the literature for telemanipulation setups. A point-to-point position mapping algorithm and a possible force mapping algorithm have been presented in [17]. Graham et al. developed in [18] a haptic feedback system that incorporates kinesthetic, vibratory, and tactile feedback for the use with a highly dexterous robotic platform. However, in most of the works presented for multi-contact applications, there is either a direct correspondence between a pair master/slave, or the master can control only a subset of the total slave DoFs.

These approaches only partially solve the problem of putting in correspondence different kinematic structures. As introduced in [19, 20, 21], it is possible to abstract from the kinematics of master/slave systems for some specific tasks, as, for instance, in cooperative manipulation. In such cases, it is possible to focus on specific parameters of a task, such as the resulting wrench applied during manipulation, instead of focusing on the contribution of the single master/slave device.

In this work, we aim to answer this question: how can master and slave devices with dissimilar kinematics (and possibly different number of interaction/contact points) be related in a bilateral telemanipulation framework? To this purpose, we have assumed that all the interaction points on the master side are actuated and can be tracked. Similarly, all the contact points on the slave side can be tracked and it is possible to measure the forces exerted. The desired abstraction from the system kinematics has been obtained defining virtual objects on the master and slave sides able to capture the motion of the operator as well as the main relevant quantities for the grasp maintenance and task execution. In [22, 23] we introduced an object-based mapping approach to map human hand synergies onto robotic hands. In this paper, we extend that framework to a telemanipulation scenario. We introduce a new algorithm to compute the force feedback when it is not possible to directly display on the master devices the forces measured at the slave side. We define as *forward mapping* the steps necessary to reproduce on the slave side the user motion captured on the master side. The *backward mapping*, instead, computes the correct forces to be displayed back to the user, starting from the measurement acquired at the slave side. The idea is pictorially represented in Fig. 1. The proposed approach is general and can be applied to different master and slave systems.

We have focused on the teleoperation of a hand/arm robotic system as a case study. Two Omega.3 devices have been used as master system, while a KUKA-KR3 arm and a five-fingered DLR-HIT Hand II have been considered as the slave hand/arm system. In [24], we presented a preliminary version of this work where only in hand manipulation was considered. The main theoretical and experimental contributions added in the present manuscript are: (i) we consider a whole hand/arm system instead of only in hand manipulation; (ii) we generalize the forward mapping to the case of n interaction points; (iii) we introduce a new strategy for backward mapping that can deal with m contact points, (iv) we introduce a passivity-based approach to ensure the stability of the system and (v) we test the teleoperation framework in two manipulation tasks.

The rest of the paper is organized as follows. In Section II the forward and backward mapping algorithms are described in detail. Section III deals with the proposed case study including a possible passivity-based solution for stability issues, while in Section IV experimental results of two possible applications are reported. Finally, in Section V conclusion and future work are outlined.

II. TELEOPERATION FRAMEWORK

A. *Forward mapping*

The way to replicate the motion of the human operator onto a robotic system has been widely investigated in the literature, see [23] for a more detailed review. In this work, we take advantage of a virtual object to abstract from the kinematics of master and slave devices. In [22] and [23] the object-based mapping initially proposed in [25] has been extended to 3D cases and to an arbitrary number of reference points necessary to define the virtual objects. In [26], the approach has been further generalized using homogeneous transformations.

In this paper, we extend the mapping with homogeneous transformations presented in [26] to the case of telemanipulation. The mapping procedure based on homogeneous transformation requires the definition of a set of interaction points on the master and a set of contact points on the slave, but lacks the definition of a specific shape for the virtual object. The virtual object used in the mapping procedure is defined by the interaction/contact points themselves. The interaction points on the master system are used to estimate a homogeneous transformation which describes the master motion. The contact points on the slave system are used to transfer this transformation on the slave device. A motion of the human hand causes a displacement of the interaction points on the master side. We assume that this transformation can be represented as a linear transformation, estimated from the displacement of the interaction points. A linear transformation matrix can be, in general, decomposed as the combination of different elementary transformations. In particular, homogeneous 4×4 matrices are widely used in computer graphics to represent the solid body transformations required to move an object and visualize it: translation, rotation, scale, shear, and perspective [27]. Any number of transformation matrices can be multiplied to form a composite matrix.

Rigid body motion is a particular type of transformation that preserves the distance between points and the angles between vectors. Rigid body motion can be represented as the combination of a rotation, defined by the rotation matrix $\mathbf{R} \in SO(3)$, and a translation motion, defined by the vector $\mathbf{p} \in \mathbb{R}^3$. The corresponding homogeneous matrix can be expressed as shown in Fig. 2a.

Homogeneous matrices can be adopted also to describe non-rigid transformations: isotropic transformations, which modify the object size by a scaling factor, without moving it; non-isotropic transformations, which modify the object size by scaling factors in the x,y, and z directions; and shear transformations, that displace each point in fixed direction, by an amount proportional to its signed distance from a line that is parallel to that direction. These basic homogeneous transformations are usually referred to as primitive transformations. A generic non-rigid transformation is qualitatively represented in Fig. 2b. In this study, we do not consider perspective transformations for the sake of simplicity. Each transformation can be represented with a more meaningful and concise representation: a scalar for the isotropic transformation, a vector for translation, 3D scaling and shear, and a quaternion for rotations. A generic linear transformation can be represented as a combination of an arbitrary number n_t of primitive transformations $\mathbf{T} = \prod_{i=1}^{n_t} \mathbf{T}_{p,i}$, where $\mathbf{T}_{p,i}$ is a generic primitive transformation. Recovering the concise form from the primitive transformation matrix is straightforward, but once primitives have been multiplied into a composite matrix, the recovery of each primitive is not usually direct. Different procedures to decompose a generic 4×4 matrix into a series of primitive transformations are available in the literature [28].

The rigid and non-rigid motions contributions from a generic linear transformation matrix can be exploited in telemanipulation. Consider, for instance, a master system tracking the human arm motion along a trajectory, while the hand is changing the grasp forces exerted onto an object. In this case, a large rigid arm displacement is coupled with a smaller non-rigid deformation. If the interaction points are placed in the human hand, their displacements contain both the contributions. In the mapping procedure it is possible to extract the rigid part of the motion from the complete transformation matrix and reproduce it with a robotic arm, while the non-rigid contribution can be replicated acting on the end-effector. In other cases, it could be interesting to reproduce only a part of the transformation on the slave. For example, while moving a grasped object from an initial to a final configuration, it could be useful to maintain constant the contact forces. To do so, only the rigid body part of the linear transformation should be replicated by the slave, while in tasks where the stability of the grasp is of primary importance, only the isotropic transformation could be replicated.

In order to consider rigid and non-rigid contributions, it is possible to express the transformation matrix as

$$\mathbf{T} = \mathbf{T}_{def}\mathbf{T}_{rb}, \tag{1}$$

where $\mathbf{T}_{rb} = \mathbf{T}_{tr}\mathbf{T}_{rot}$ represents the rigid part of the displacement, composed of a rotation and a translation, and $\mathbf{T}_{def}$ takes into account the non-rigid deformation. The extraction of the translation part of the rigid body motion from the starting matrix $\mathbf{T}$ is straightforward, while for the non rigid part the reader is referred to [29].

In the following, we summarize how to estimate the linear transformation matrix $\mathbf{T}$ from the motion of the interaction points on the master side and how it is mapped on the slave side when no hypotheses regarding its decomposition are assumed (most general case).

Let $\{W_m\}$ be a reference frame attached to the master system and $\{W_s\}$ a reference frame adopted to describe the slave motion. Let us define the vector $\mathbf{p}^m \in \mathbb{R}^{3n^m}$ as the collections of all the $\mathbf{p}_j^m \in \mathbb{R}^3$ interaction points on the master, where $j = 1, \cdots, n^m$ with n^m the number of interaction points. Similarly, a set of n^s contact points are defined on the slave, indicated with $\mathbf{p}_l^s$, with $l = 1, \cdots, n^s$. Note that, in general, $n^m \neq n^s$, and n^m and n^s are not a priori related.

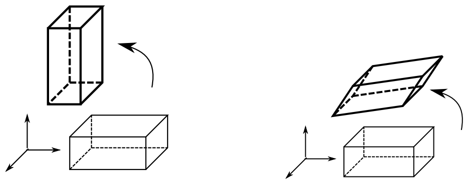

$$\mathbf{T}_{rb} = \begin{bmatrix} \mathbf{R} & p \\ 0 & 1 \end{bmatrix} \qquad \mathbf{T}_{def} = \begin{bmatrix} 1 & h_{xy} & h_{xz} & 0 \\ h_{yx} & 1 & h_{yz} & 0 \\ h_{zx} & h_{zy} & 1 & 0 \\ 0 & 0 & 0 & 1 \end{bmatrix}$$

(a) (b)

Fig. 2. Examples of linear transformations applied to a cube and corresponding homogeneous matrices: (a) rigid body motion, (b) shear and scale transformation.

Let us define $\hat{\mathbf{p}}_{j,i}^m \in \mathbb{R}^4$ as the augmented representation of the coordinates of the generic interaction point $\mathbf{p}_j^m$ when the master is in a given initial configuration and $\hat{\mathbf{p}}_{j,f}^m \in \mathbb{R}^4$ the augmented representation of coordinates of $\mathbf{p}_j^m$ in a given final configuration[1].

The forward mapping procedure is based on the hypothesis that, for each point $\mathbf{p}_j^m$, with $j = 1, \cdots, n^m$, the following linear equation holds

$$\hat{\mathbf{p}}_{j,f}^m = \mathbf{T}\hat{\mathbf{p}}_{j,i}^m, \tag{2}$$

where $\mathbf{T} \in \mathbb{R}^{4\times4}$ is a linear transformation. For a given motion of the interaction points on the master side, i.e., for a given set of initial and final positions of the interaction points $\hat{\mathbf{p}}_{j,i}^m$ and $\hat{\mathbf{p}}_{j,f}^m$, the $\mathbf{T}$ matrix can be evaluated by solving the following linear system

$$\hat{\mathbf{p}}_f^m = \mathbf{\Lambda}\mathbf{t}, \tag{3}$$

in which the vector $\mathbf{t} \in \mathbb{R}^{12}$ contains the components of the linear transformation $\mathbf{T}$, the matrix $\mathbf{\Lambda} \in \mathbb{R}^{3n^m \times 12}$ depends on $\hat{\mathbf{p}}_{j,f}^m$ and $\hat{\mathbf{p}}_f^m$ collects all the points in the final configuration. See [26] for more details on the computation of matrix $\mathbf{\Lambda}$.

The main idea behind the proposed forward mapping procedure is that a homogeneous matrix $\mathbf{T}_{sl}$ computed on the basis of the matrix estimated on the master is used to update the position of the contact points on the slave. According to the specific implementation and requirements, the matrix $\mathbf{T}_{sl}$ could be equal to $\mathbf{T}$, in case scaled, or, using a specific decomposition technique, divided in two or more primitive transformations, or simplified to take into account only a part of the deformation. Assume that in the initial reference configuration, the coordinates of the contact points on the slave are $\mathbf{p}_{l,i}^s$, collected in the vector $\mathbf{p}_i^s$. The final configuration of these points, according to the above defined linear transformation, can be evaluated as

$$\hat{\mathbf{p}}_{l,f}^s = \mathbf{T}_{sl}\,\hat{\mathbf{p}}_{l,i}^s. \tag{4}$$

---

[1] Given a generic three-dimensional vector $\mathbf{a}$, $\hat{\mathbf{a}} \in \mathbb{R}^4$ is the augmented representation adopted to write affine transformations, i.e., $\hat{\mathbf{a}} = [\mathbf{a}\ 1]^T$.

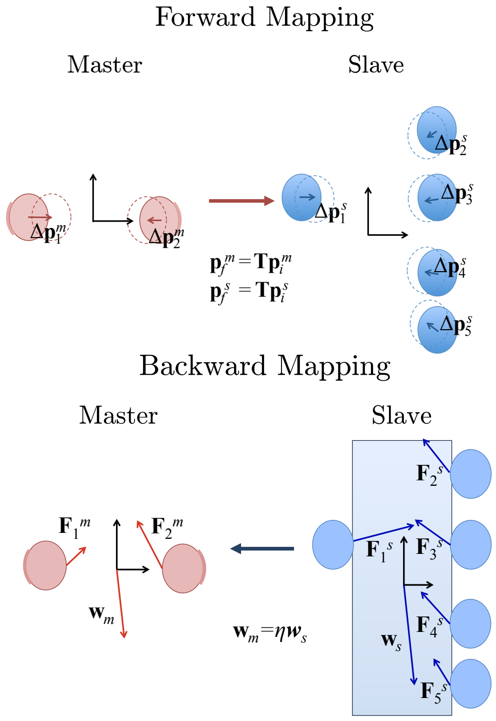

Fig. 3. Concept of forward and backward mappings. As example, two interaction points are considered on the master side and five contact points are considered on the slave side. In the forward mapping, the same homogeneous transformation $\mathbf{T}$ evaluated on the master side is replicated on the slave side. In the backward mapping, the wrench $\mathbf{w}_s$ applied on the object grasped by the slave system is considered to act, possibly scaled, also on the virtual object defined on the master side and adopted to evaluate the forces to be rendered.

Once the final configuration of the reference points on the slave side $\hat{\mathbf{p}}_{l,f}^s$ has been defined, their values are sent to the slave control system that updates the contact points position through a suitable inverse kinematic strategy, depending on the robotic system structure. In Section III, we describe the application of this procedure to a slave system composed of a robotic arm and a multi-fingered hand.

Remark 1: The forward mapping presented in this work is general and can be used to put in correspondence master and slave devices with very dissimilar kinematics and possibly with a different number of interaction/contact points. The possibility that the overall grasp conditions on the master and slave sides of the system are different exists, for example, if the master side has three interaction points and the slave grasps an object with two contact points without torsional friction. In this case, the grasp at the slave side is under-determined, and this condition has to be effectively communicated to the master. In this paper, we did not consider this possibility for the sake of conciseness. However, this event can be communicate to the operator on the master side using additional haptic channels, for example through vibrating wearable devices, or with visual/acoustic warning signals.

B. Backward mapping

In the following, we describe the backward mapping procedure, i.e., how to evaluate the forces to be rendered by each master device starting from the contact forces measured on the slave side. The backward mapping is the key concept of the proposed bilateral teleoperation framework between different kinematic structures.

Let us assume that the slave system grasps an object through n^s contact points. Assume also that the position of the contact points are tracked and the contact forces measured. Let $\mathbf{F}^s \in \mathbb{R}^{3n^s}$ be defined as the collection of forces $\mathbf{F}_l^s \in \mathbb{R}^3$ with $l = 1, \dots, n^s$ measured at the contact points at the slave.

The wrench acting on the slave side, $\mathbf{w}_s \in \mathbb{R}^6$, is computed as

$$\mathbf{w}_s = -\mathbf{G}_s\, \mathbf{F}^s,$$

where $\mathbf{G}_s \in \mathbb{R}^{6\times 3n^s}$ is the grasp matrix, evaluated for the contact points on the slave system. For a complete discussion on grasp matrix definition, the reader is referred to [30, 31].

We can decompose the $\mathbf{F}^s$ contact forces in external and internal forces, i.e., $\mathbf{F}^s = \mathbf{F}_e^s + \mathbf{F}_i^s$, where

$$\mathbf{F}_e^s = \mathbf{G}_s^{\#}\mathbf{G}_s\mathbf{F}^s$$

is the projection of $\mathbf{F}^s$ vector onto the image of $\mathbf{G}_s$ (external forces) and

$$\mathbf{F}_i^s = (\mathbf{I} - \mathbf{G}_s^{\#}\mathbf{G}_s)\mathbf{F}^s \tag{5}$$

is the projection of $\mathbf{F}^s$ vector onto $\mathcal{N}(\mathbf{G}_s)$ (internal forces) [32], where the symbol $\mathcal{N}(\bullet)$ indicates the kernel of a generic matrix $\bullet$ and the symbol $^{\#}$ represents the pseudo-inverse operator.

The definition of a virtual object on the master system allows us to assume the following relation: the total wrench $\mathbf{w}_s$ acting on the object grasped by the slave system is also acting on the virtual object defined for the master, possibly scaled. Consequently, we assume

$$\mathbf{w}_m = \eta\, \mathbf{w}_s, \tag{6}$$

where $\mathbf{w}_m \in \mathbb{R}^6$ is the wrench acting on the virtual object in the master side (see Fig. 3), while the scale factor η takes into account the maximum force constraints of the actuators on the master/slave system. This equation can be rewritten in terms of contact forces as

$$\mathbf{G}_m\, \mathbf{F}^m = \eta\, \mathbf{G}_s\, \mathbf{F}^s, \tag{7}$$

where $\mathbf{G}_m \in \mathbb{R}^{6\times 3n^m}$ is the grasp matrix defined for the master system and $\mathbf{F}^m \in \mathbb{R}^{3n^m}$ is the collection of the forces $\mathbf{F}_j^m \in \mathbb{R}^3$ with $j = 1, \dots, n^m$ to be actuated on the master side. Vector $\mathbf{F}^m$ in Eq. (7) can be computed as

$$\mathbf{F}^m = \eta(\mathbf{F}_e^m + \mathbf{F}_i^m), \tag{8}$$

where the particular non-homogeneous solution, i.e., the set of contact forces whose resulting wrench is $\mathbf{w}_m$, referred to as external forces, is given by

$$\mathbf{F}_e^m = \mathbf{G}_m^{\#}\, \mathbf{G}_s\, \mathbf{F}^s, \tag{9}$$

and the general solution of the homogeneous problem, i.e., the internal forces, are evaluated as

$$\mathbf{F}_i^m = \mathbf{N}_{Gm}\, \boldsymbol{\zeta}\,, \tag{10}$$

where $\mathbf{N}_{Gm}$ is a matrix whose columns form a basis for $\mathcal{N}(\mathbf{G}_m)$ and $\boldsymbol{\zeta} \in \mathbb{R}^m$ is a vector parameterizing the homogeneous part of the solution. While the non-homogeneous part of the solution, Eq. (9), is straightforward, how to tune the homogeneous part, Eq. (10), represents an issue. In general, the solution is not unique and it is necessary to determine the direction where it is more convenient to render the forces. The value of ζ could be selected considering the human hand skills in terms of joint torques and muscle activity. In [33], for instance, the authors investigated which direction minimizes the torque exerted by the hand during a three-finger grasp. They demonstrated that in this type of grasps humans try to reduce the effort by choosing the contact force direction properly. The value of ζ could be also selected considering the minimization of a cost function, for example the function defined in [32], to evaluate the optimal choice of grasping forces. The main drawback of these approaches is that the obtained mapping does not depend on the action of the human at the master side, but it is a priori chosen.

TABLE I
FEATURES OF THE DEVICES COMPOSING THE BILATERAL TELEMANIPULATION SYSTEM.

Omega.3	Manufacturer	Force Dimension, CH
	workspace (translation)	$\varnothing 160\times 110$ mm
	forces (translation)	12.0 N
	resolution (translation)	<0.01 mm
	stiffness (closed-loop)	14.5 N/mm
	refresh rate	up to 4 KHz
	structure	delta-based parallel kinematics with active gravity compensation
KR3	Manufacturer	KUKA, GE
	# of Axes	6
	Load Capacity	3 kg
	Reach	635 mm
	Repeatability	0.05 mm
	Robot Mass	53 kg
DLR-HIT Hand II	Manufacturer	DLR (GE) & HIT (PRC)
	# identical fingers	5
	Fingers joints	4 joints
	Fingers DoF	3 (last two joints are mechanically coupled with a transmission ratio 1:1)
	Joint position sensors	one per joint
	Joint torque sensors	one per joint
	Weight	1.5 kg
	Fingertip force	up to 10 N
	Proximal phalanx	Length - 55 mm Width - 20 mm
	Middle phalanx	Length - 25 mm Width - 20 mm
	Distal phalanx	Length - 25 mm Width - 19.2 mm
	Base joint	Length - 64.1 mm Width - 24.7 mm

III. CASE STUDY

A. Experimental setup

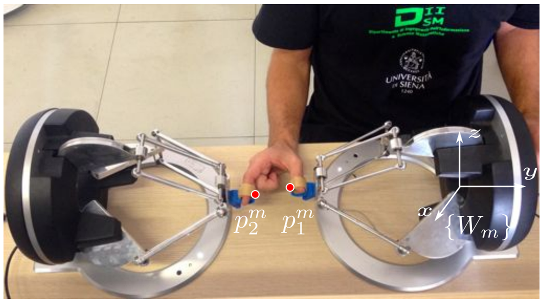

Fig. 4. Master subsystem. The two Omega.3 haptic devices are equipped with 3D printed thimbles to easily fit the human fingers. $\mathbf{p}_1^m$ and $\mathbf{p}_2^m$ indicate the position of the haptic interfaces end-effectors in the $\{W_m\}$ reference frame.

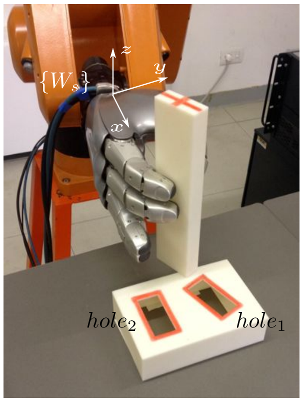

Fig. 5. Slave subsystem. A DLR-HIT Hand II is connected to a KUKA-KR3 arm. The reference frame of the slave system is located at the wrist.

Two Omega.3 haptic devices define the master side, while a DLR-HIT Hand II mounted on a KUKA KR3 arm form the hand/arm system at the slave side. Please refer to Tab. I for further information about the considered hardware specifications. The haptic interfaces are equipped with a custom 3D printed thimble, instead of the default end-effector, to easily fit the human fingertip (see Fig. 4).

As introduced in Sec. II, we consider a single reference frame for the master side $\{W_m\}$. A preliminary calibration procedure is carried out to place the devices in the correct positions, making coherent the whole master side in terms of reference frames. The peg position is computed with respect to the reference frame $\{W_s\}$, placed on the wrist of the arm, as shown in Fig. 5.

A multi-thread software is built to let the heterogeneous interfaces communicate together and manage the difference in terms of sampling rate.

The master and slave systems are connected to the same Local Area Network (LAN). However, thanks to the underlying communication infrastructure, they could have easily been placed in different LANs and then communicate through an Internet connection.

B. Telemanipulation framework for the case study

The telemanipulation framework proposed in Section II is general and can be used considering different devices as master and slave systems. In this specific case study, we have a system – the multi-fingered hand – that is able to stably grasp an object, but it has a small workspace volume and limited manipulability capabilities, and another system – the arm – whose workspace is larger. If we consider a task in which the slave system is asked to grasp and move an object, the role of the hand could be to assure the stability of the grasp during the task, while the role of the arm could be mainly to realize the re-positioning motion. In this case, it is possible to separately manage the rigid body motion of the teleoperated object and the tightness of the grasp (i.e., the non-rigid deformation).

To this aim, in the forward mapping the transformation matrix $\mathbf{T}$ defined in Eq. (2) can be furthermore decomposed as

$$\mathbf{T} = \mathbf{T}_{def}\mathbf{T}_{rb},$$

where $\mathbf{T}_{def}$ represents the non-rigid part of the transformation (i.e., the squeezing action), and $\mathbf{T}_{rb}$ is a rigid-body transformation, as introduced in Section II-A. According to this decomposition of $\mathbf{T}$, the motion of the contact points on the master system is represented as the composition of two distinct linear transformations

$$\hat{\mathbf{p}}^m_{j,rb} = \mathbf{T}_{rb}\hat{\mathbf{p}}^m_{j,i}, \quad \hat{\mathbf{p}}^m_{j,f} = \mathbf{T}_{def}\hat{\mathbf{p}}^m_{j,rb},$$

where $\hat{\mathbf{p}}^m_{j,rb}$ is the configuration that the point would reach if we considered only the rigid body part of the transformation. We can therefore introduce the displacement

$$\mathbf{\Delta p}^m_j = \mathbf{p}^m_{j,f} - \mathbf{p}^m_{j,i} = \mathbf{\Delta p}^m_{j,rb} + \mathbf{\Delta p}^m_{j,def}, \qquad (11)$$

where $\mathbf{\Delta p}^m_{j,rb} = \mathbf{p}^m_{j,rb} - \mathbf{p}^m_{j,i}$, $\mathbf{\Delta p}^m_{j,def} = \mathbf{p}^m_{j,f} - \mathbf{p}^m_{j,rb}$.

Assume that in the initial reference configuration the coordinates of the contact points on the slave are $\mathbf{p}^s_{l,i}$, collected in the vector $\mathbf{p}^s_i$. The final configuration of these points, according to the above defined linear transformation, can be evaluated as the composition of two motions

$$\hat{\mathbf{p}}^s_{l,f} = \mathbf{T}_{def}\mathbf{T}_{rb}\hat{\mathbf{p}}^s_{l,i}. \qquad (12)$$

The l-th contact point after the rigid transformation defined by matrix $\mathbf{T}_{rb}$ can be denoted by $\mathbf{p}^s_{l,rb} \in \mathbb{R}^3$, leading to the following relation

$$\hat{\mathbf{p}}^s_{l,f} = \mathbf{T}_{def}\hat{\mathbf{p}}^s_{l,rb}. \qquad (13)$$

Collecting all the $\mathbf{p}^s_{l,rb}$ in the vector $\mathbf{p}^s_{rb} \in \mathbb{R}^{3n^s}$ and all the final points $\mathbf{p}^s_{l,f}$ in the vector $\mathbf{p}^s_f \in \mathbb{R}^{3n^s}$ and introducing two scaling factors α and β to mitigate possible differences between the size of master and slave workspaces, we can define the displacements $\mathbf{\Delta p}^s_{rb} \in \mathbb{R}^{3n^s}$ and $\mathbf{\Delta p}^s_{def} \in \mathbb{R}^{3n^s}$ as

$$\mathbf{\Delta p}^s_{rb} = \alpha(\mathbf{p}^s_{rb} - \mathbf{p}^s_i) \qquad \mathbf{\Delta p}^s_{def} = \beta(\mathbf{p}^s_f - \mathbf{p}^s_{rb}). \qquad (14)$$

Remark 2: Displacements $\mathbf{\Delta p}^s_{rb}$ and $\mathbf{\Delta p}^s_f$ are the displacements to be imposed to the slave contact points. As described in Section III-C, these values are kept only when they do not violate the passivity constraints adopted to stabilize the system. When necessary, scaled versions $\mathbf{\Delta \bar{p}}^s_{rb} \in \mathbb{R}^{3n^s}$ and $\mathbf{\Delta \bar{p}}^s_{def} \in \mathbb{R}^{3n^s}$ are computed by the passivity layer to ensure the stability of the loop.

The rigid body displacement $\mathbf{\Delta \bar{p}}^s_{rb}$ is then mapped to the arm wrist displacement $\mathbf{\Delta u}^s_{rb} \in \mathbb{R}^6$ through the matrix $\mathbf{B} \in \mathbb{R}^{6\times 3n^s}$. The displacement $\mathbf{\Delta \bar{p}}^s_{def}$ due to the non-rigid part is obtained acting on the robotic hand joint values, according to robotic hand inverse kinematics. If the displacement $\mathbf{\Delta \bar{p}}^s_{def}$ is sufficiently small, the linear approximation of the kinematics of the robot can be considered. Consequently, the displacement that has to be imposed to the robotic hand joints $\mathbf{q}_r$, can be evaluated as

$$\mathbf{\Delta q}^s_{def} = \mathbf{J}^{\#}_r \mathbf{\Delta \bar{p}}^s_{def} + \mathbf{N}_{J_r}\boldsymbol{\varrho}, \qquad (15)$$

where $\mathbf{J}_r$ is the robotic hand Jacobian matrix, $\mathbf{N}_{J_r}$ is a basis of the $\mathbf{J}_r$ nullspace and $\boldsymbol{\varrho}$ is a vector parametrizing the homogeneous part of the inverse differential kinematics problem and managing the presence of redundant DoFs [31].

The displacement decomposition in Eq. (11), is exploited also for the backward mapping. As mentioned in Section II-B, the computation of the homogeneous part of the solution of Eq. (10) has to take into account the action of the human operator on the master side. According to the quasi static model presented in [34], it is possible to verify that, assuming that the operator's hand on the the master side is grasping a virtual object with a finite stiffness at the contacts described by matrix $\mathbf{K_v} \in \mathbb{R}^{3n^m\times 3n^m}$, symmetric and positive definite, the contact force variation induced by the non-rigid part of the displacement $\mathbf{\Delta p}^m_{def} = [\mathbf{\Delta p}^{m\mathrm{T}}_{1,def}, \cdots, \mathbf{\Delta p}^{m\mathrm{T}}_{n^m,def}]^{\mathrm{T}} \in \mathbb{R}^{3n^m}$ of the interaction points leads to a variation of the virtual contact forces

$$\mathbf{\Delta F}^m_{v,i} = \left(\mathbf{I} - \mathbf{G}^{\#}_{m,K}\mathbf{G}_m\right)\mathbf{K}_v\mathbf{\Delta p}^m_{def}, \qquad (16)$$

where $\mathbf{G}^{\#}_{m,K} = \mathbf{G}^{\mathrm{T}}_m(\mathbf{G}_m\mathbf{K}_v\mathbf{G}^{\mathrm{T}}_m)^{-1}$ is the $\mathbf{K}_v$-weighted pseudoinverse of $\mathbf{G}_m$. It is possible to verify that $\mathbf{F}^m_{v,i} \in \mathcal{N}(\mathbf{G_m})$, which means that the computed contact forces do not influence the equivalent wrench $\mathbf{w}_m$ [34]. Eq. (16) transforms a motion of the user's fingertips in a virtual contact force, through the stiffness matrix $\mathbf{K}_v$. This force is then projected onto the nullspace of the grasp matrix $\mathbf{G}_m$ to obtain a set of contact forces that do not affect the wrench $\mathbf{w}_m$. The contact forces evaluated in Eq. (16) neglect the actual contact forces measured on the slave side. Such forces are only used to compute the directions in which internal forces have to be displayed on the master side. The magnitude of internal forces rendered on master side are then scaled according to the magnitude of the internal forces at the slave side $\mathbf{F}^s_i$ as

$$\mathbf{F}^m_i = \frac{\mathbf{\Delta F}^m_{v,i}}{\|\mathbf{\Delta F}^m_{v,i}\|}\frac{1}{n^m}\sum_{l=1}^{n^s}\|\mathbf{F}^s_{i,l}\|. \qquad (17)$$

Remark 3: As for the forward mapping, also the output of the backward mapping $\mathbf{F}^m$ is modulated by the passivity layer, if needed, to keep the system passive. In Section III-C, $\bar{\mathbf{F}}^m \in \mathbb{R}^{3n^m}$ will be computed as the set of feedback forces effectively applicable on the master side, without violating the passivity constraints.

Remark 4: In the proposed approach, the information about the total applied wrench is privileged with respect to information at the single contact point force contribution. This abstraction is necessary to consider different kinematics and a different number of interaction points between master interfaces and slave robots. The rendered forces on master side are, thus, not informative of the single contact situation at the slave side. However, if a contact is broken the total amount of rendered internal forces decreases so giving indirect information about the contacts situation.

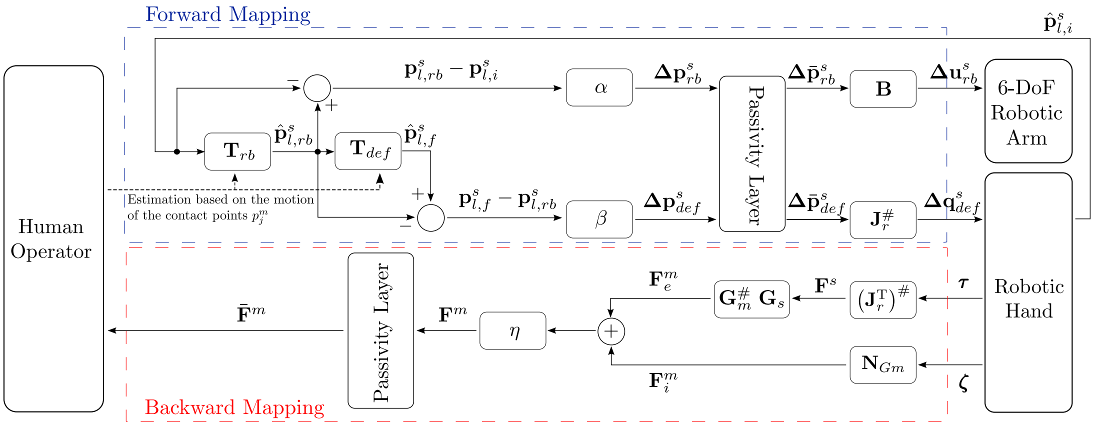
Forward Mapping
$\hat{\mathbf{p}}^s_{l,i}$
$\mathbf{p}^s_{l,rb} - \mathbf{p}^s_{l,i}$
$-$
$+$
α
$\Delta\mathbf{p}^s_{rb}$
Passivity Layer
$\Delta\bar{\mathbf{p}}^s_{rb}$
$\mathbf{B}$
$\Delta\mathbf{u}^s_{rb}$
6-DoF Robotic Arm
Human Operator
$\mathbf{T}_{rb}$
$\hat{\mathbf{p}}^s_{l,rb}$
$\mathbf{T}_{def}$
$\hat{\mathbf{p}}^s_{l,f}$
Estimation based on the motion of the contact points p^m_j
$+$
$-$
$\mathbf{p}^s_{l,f} - \mathbf{p}^s_{l,rb}$
β
$\Delta\mathbf{p}^s_{def}$
$\Delta\bar{\mathbf{p}}^s_{def}$
$\mathbf{J}^{\#}_r$
$\Delta\mathbf{q}^s_{def}$
Robotic Hand
$\mathbf{F}^m_e$
$\mathbf{G}^{\#}_m\ \mathbf{G}_s$
$\mathbf{F}^s$
$(\mathbf{J}^{\mathrm{T}}_r)^{\#}$
$\boldsymbol{\tau}$
$\bar{\mathbf{F}}^m$
Passivity Layer
$\mathbf{F}^m$
η
$\mathbf{N}_{Gm}$
$\boldsymbol{\zeta}$
$\mathbf{F}^m_i$
Backward Mapping

Fig. 6. Schematic overview of the proposed bilateral telemanipulation framework. The *forward mapping* defines how to move a remote robotic hand and a remote robotic arm using a homogeneous matrix $\mathbf{T} = \mathbf{T}_{rb}\,\mathbf{T}_{def}$ computed at the human operator side. Through the *backward mapping* forces measured by the slave system are rendered on the haptic interfaces at the master side.

Finally, in the DLR-HIT Hand II it is not possible to read the forces at the contact points if additional force sensors are not considered. However, it is possible to estimate the contact forces starting from the torques $\boldsymbol{\tau}$ measured at the joints through the torque sensors embedded in the device. Forces at the contact points $\mathbf{F}^s$ are thus estimated considering

$$\mathbf{F}^s = (\mathbf{J}^{\mathrm{T}}_r)^{\#}\,\boldsymbol{\tau} + \mathbf{N}_{J^{\mathrm{T}}_r}\,\boldsymbol{\chi}\ , \tag{18}$$

where $\mathbf{J}_r$ is the Jacobian matrix of the slave system, $\mathbf{N}_{J^{\mathrm{T}}_r}$ is a matrix whose columns form a basis of $\mathcal{N}(\mathbf{J}^{\mathrm{T}}_r)$, and the vector $\boldsymbol{\chi}$ parametrizes the homogeneous solution to the equilibrium problem [30, 31]. The estimation is straightforward in case of trivial $\mathcal{N}(\mathbf{J}^{\mathrm{T}}_r)$ as in our experimental setup, where the slave has three joints for each finger and the contact point is at the fingertip. More complex model-based estimations must be assumed when $\mathcal{N}(\mathbf{J}^{\mathrm{T}}_r)$ is not trivial.

The complete scheme of the telemanipulation framework for the case study is reported in Fig. 6.

C. Passivity layer for multi-contact interaction

In this section, the passivity-based solution adopted to ensure the stability of the proposed teleoperation loop is described. Guaranteeing the passivity of a system is a sufficient condition to ensure its stability [35]. A system can be defined as *passive* if the energy that can be extracted from it is bounded by the sum of the injected and the initial stored energy. The interaction between passive systems is guaranteed to be stable, and any proper combination of these systems leads to a passive system again [36]. Without any assumption on the teleoperation system, its energy balance can be expressed as the sum of the energy stored in all its components. The total energy H_t of the system at instant t can be written as

$$H_t(t) = H_m(t) + H_s(t) + H_c(t), \tag{19}$$

where $H_m(t)$, $H_s(t)$, and $H_c(t)$ represent the energy stored at the instant t on the master system, on the slave system and in the communication channel, respectively. The passivity condition for the system can be thus expressed by

$$H_t(t) \geq 0, \tag{20}$$

assuming that the initial energy stored in the system is zero.

Master and slave systems only exchange physical energy with the user and with the environment, respectively. A passive interconnection of the entire teleoperation system can be then ensured if the following inequality holds

$$\dot{H}_t(t) \leq P_m(t) + P_s(t), \tag{21}$$

where $P_m(t)$ is the power flowing from the master system to its controller, $P_s(t)$ is the power flowing from the slave system to its controller, and $\dot{H}_t(t)$ is the rate of change of $H_t(t)$.

Several approaches have been developed to make a teleoperation system satisfy the inequalities (20) and (21), e.g., Scattering Algorithm [37], Time Domain Passivity Control [38], Energy Bounding Algorithm [7] and Passive Set Position Modulation [4].

In [6], a dual-layer controller structure has been presented. A *transparency layer* is in charge of computing the ideal forces to be actuated in both the master and the slave systems without considering any passivity constraint. At the same time, a *passivity layer* modulates these forces, if needed, to avoid violations of passivity conditions, ensuring the stability of the system at the price of a temporary loss of transparency. The key element of this algorithm is the definition of two *tanks*, one for the master and one for the slave. The tanks can be seen as communicating energy storage units from which the motions of master and slave are powered. Separate communication channels connect the layers at the slave and master levels so that information related to exchanged energy is separated from information about the desired behavior. This feature leads to a level of generality that makes possible to build the passivity layer on top of any transparency layer, regardless of the specific algorithm used to compute the ideal forces.

In this work, we implemented a two-layer approach to guarantee the stability of our teleoperation framework, taking inspiration from [6]. Fig. 7 graphically represents the role of the passivity layer implemented. Forward and backward mappings, seen as parts of a unique transparency layer, generate displacements and feedback forces respectively. The passivity layer generates scaled versions of the computed quantities to fulfill the constraint in Eq. (21). The application of the two-layer approach presented in [6] to a multi-contact

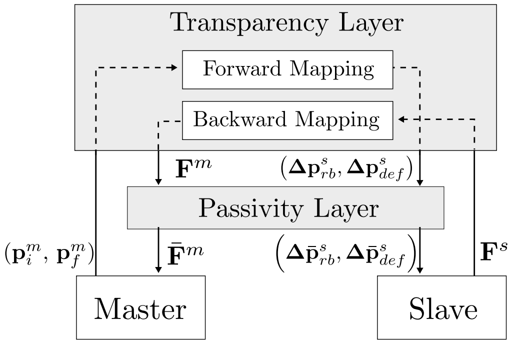
Transparency Layer
Forward Mapping
Backward Mapping
$\mathbf{F}^m$
$(\boldsymbol{\Delta}\mathbf{p}^s_{rb}, \boldsymbol{\Delta}\mathbf{p}^s_{def})$
Passivity Layer
$(\mathbf{p}^m_i, \mathbf{p}^m_f)$
$\bar{\mathbf{F}}^m$
$(\boldsymbol{\Delta}\bar{\mathbf{p}}^s_{rb}, \boldsymbol{\Delta}\bar{\mathbf{p}}^s_{def})$
$\mathbf{F}^s$
Master
Slave

Fig. 7. Block diagram of the implemented two-layer approach that ensures the passivity of the teleoperation framework.

telemanipulation context is one of the contributions of this paper.

In the proposed framework, time delays associated to the communication channel are assumed to be negligible, since the network connecting master and slave subsystems is wired and local. In these cases, a simplified version of the two-layer approach, detailed in [6], can be implemented. A delay-free channel in the passivity layer ensures an instantaneous communication and can be considered as a physical interconnection between the two tanks. Two physically interconnected tanks substantially behave as a single tank that stores the energetic contributions of both master and slave. A single tank was, thus, associated to the whole teleoperation loop. In the following, how the proposed passivity layer works will be explained in detail.

Let us define the energy level $H(t)$ of the tank (associated to the whole loop) at the generic time instant t as

$$H(t) = H_m(t) + H_s(t). \tag{22}$$

At each time step both master and slave systems perform dissipative or non-dissipative actions extracting/adding energy from/to the tank (decreasing or increasing the value of H).

Firstly, let us consider the master side. Let ΔT_m be the length of the master sampling period. The energy variation $\Delta H_m(k)$ that occurs on the master side at the generic sampling step k can be computed as

$$\Delta H_m(k) = \sum_{j=1}^{n_c^m} \int_{(k-1)\Delta T_m}^{k\Delta T_m} \mathbf{F}_j^m(k-1) \cdot \dot{\mathbf{p}}_j^m(t)dt, \tag{23}$$

where "$\cdot$" denotes the dot (scalar) product between vectors. Note that the forces actuated on the master side $\mathbf{F}_j^m(k) \in \mathbb{R}^3$ with $j = 1, \ldots, n^m$ are assumed to be constant during a sampling period. The energy variation $\Delta H_m(k)$ is negative if the action performed by the master during a sampling interval is dissipative, while $\Delta H_m(k)$ is positive in case of a non-dissipative action. The tank level must be updated, at each step, to take into account this energy variation

$$H(k+1) = H(k) + \Delta H_m(k). \tag{24}$$

On the slave side the energy variation $\Delta H_s(k)$ can be similarly computed as

$$\Delta H_s(k) = \sum_{l=1}^{n_c^s} \int_{(k-1)\Delta T_s}^{k\Delta T_s} \mathbf{F}_l^s(k-1) \cdot \dot{\mathbf{p}}_k^s(t)dt, \tag{25}$$

where ΔT_s is the length of the slave sampling period. Also in this case, the forces $\mathbf{F}_l^s(k) \in \mathbb{R}^3$ with $l = 1, \ldots, n^s$ exerted by the robot on the environment are assumed to be constant during a sampling period. The same considerations on the sign of $\Delta H_m(k)$ can be replicated for $\Delta H_s(k)$.

After each action performed by the slave, the level of H must be updated as well as

$$H(k+1) = H(k) + \Delta H_s(k). \tag{26}$$

The passivity layer limits the displacement that can be imposed to the robotic hand/arm system in order to avoid unstable behaviors of the system. Starting from the ideal displacements $\boldsymbol{\Delta}\mathbf{p}^s_{rb}$ and $\boldsymbol{\Delta}\mathbf{p}^s_f$ computed by the transparency layer, two scaled displacements $\boldsymbol{\Delta}\bar{\mathbf{p}}^s_{rb}$ and $\boldsymbol{\Delta}\bar{\mathbf{p}}^s_f$ are then computed and imposed to the robot, preserving the passivity of the loop, as

$$\boldsymbol{\Delta}\bar{\mathbf{p}}^s_{rb} = \frac{\boldsymbol{\Delta}\mathbf{p}^s_{rb}}{\|\boldsymbol{\Delta}\mathbf{p}^s_{rb}\|} \min(\|\boldsymbol{\Delta}\mathbf{p}^s_{rb}\|, \Delta p^{lim}_{rb}) \tag{27}$$

$$\boldsymbol{\Delta}\bar{\mathbf{p}}^s_{def} = \frac{\boldsymbol{\Delta}\mathbf{p}^s_{def}}{\|\boldsymbol{\Delta}\mathbf{p}^s_{def}\|} \min(\|\boldsymbol{\Delta}\mathbf{p}^s_{def}\|, \Delta p^{lim}_{def}), \tag{28}$$

where Δp^{lim}_{rb} and Δp^{lim}_{def} are defined on the basis of H as

$$\Delta p^{lim}_{rb} = \frac{H}{n^s \Delta F^{max}_{rb}} \qquad \Delta p^{lim}_{def} = \frac{H}{n^s \Delta F^{max}_{def}}. \tag{29}$$

The parameters $\Delta F^{max}_{rb} \in \mathbb{R}$ and $\Delta F^{max}_{def} \in \mathbb{R}$ are estimations of the norms of the maximum variations of external and internal forces respectively, that can be exerted by the robot at a single contact point during a sampling step. They can be arbitrarily set as parameters of the passivity layer.

Remark 5: Passivity constrains are computed on the displacement of contact points both for rigid and non-rigid motions, although rigid body motions are then executed with the arm. If a force/torque sensor was present on the robot wrist, it would be possible to limit the displacement directly at the arm level.

The forces $\mathbf{F}^m$ computed in the transparency layer by the mapping algorithm (according to Eq. (8)) are modulated, if needed, as it follows. Let us define $\mathbf{F}^m_{PL} \in \mathbb{R}^{3n^m}$ as the set of forces that can be effectively provided to the human user while preserving the passivity of the loop. Depending on the value of H, such forces are a scaled version of $\mathbf{F}^m$ and can be computed as

$$\mathbf{F}^m_{PL} = \frac{\mathbf{F}^m}{\|\mathbf{F}^m\|} \min(\|\mathbf{F}^m\|, F^{lim}), \tag{30}$$

where F^{lim} is defined as

$$F^{lim} = \frac{H}{n^m \Delta p^{max}}. \tag{31}$$

The parameter Δp^{max} belongs to the arbitrary choices of the passivity layer and represents an estimation of the maximum displacement that can be observed on the master side, at each interaction point, during a single sampling step.

The master and slave motions commanded by the transparency layer influence the quantity of energy flowing into or out of the teleoperation loop. The system described so far can theoretically drive the energy level H to zero, due to a number of dissipative actions performed on the master and slave sides. In order to completely decouple the two layers, a method is required to regulate the level of H independently from the actions commanded by the transparency layer, as described in [6]. With this aim, a tank level controller (TLC) is introduced on the master side. This controller regulates the level H to a desired level H_d as it follows. At each sample step k, if the level $H(k)$ is lower than H_d, a small additional amount of energy is extracted from the user during the next sampling period $k+1$ to refill the tank. A possible implementation of the TLC controller can be represented by a modulated viscous damper which applies a small opposing force $\mathbf{F}^m_{TLC} \in \mathbb{R}^{3n^m}$ to the user. Such force is defined as

$$\mathbf{F}^m_{TLC} = -d(k)\dot{\mathbf{p}}^m, \tag{32}$$

where

$$d(k) = \begin{cases} \nu(H_d - H(k)) & \text{if } H(k) < H_d \\ 0 & \text{otherwise} \end{cases}, \tag{33}$$

with $\nu \in \mathbb{R}$ arbitrary set as parameter of the passivity layer. The force $\mathbf{F}_{TLC}$ is thus added to $\mathbf{F}_{PL}$ to get the final force applied by the master device on the user as

$$\bar{\mathbf{F}}^m = \mathbf{F}^m_{PL} + \mathbf{F}^m_{TLC}. \tag{34}$$

IV. EXPERIMENTAL RESULTS

We evaluated the performance of the proposed telemanipulation framework considering two different tasks: peg in a hole and LEGO bricks assembly. Both tasks required fine manipulation skills and a fine control of exerted forces that were possible using our bilateral teleoperation system.

A. Peg in a hole

The task consisted in picking a peg from a hole in the support base and placing it inside another one with a different orientation (see Fig. 5). The peg was a 3D-printed parallelepiped with a 2×5 cm base and 20 cm height. The size of the holes in the support base was 2.5×5.5 cm, while the board was 3.5 cm high. The starting hole ($hole_1$) was rotated of 20 degrees with respect to the final hole ($hole_2$) about the direction perpendicular to the punctured board surface. This choice was adopted to highlight the capability of the system in reproducing wrist rotations. We performed a three-finger grasp with the robotic hand involving thumb, index, and middle fingers.

Fig. 8 shows the trajectories of the virtual object centers, defined both at the master and slave sides, projected on the $z-y$ plane. On both the master and slave sides, the virtual object centers $\mathbf{o}_m$ and $\mathbf{o}_s$ are considered as the mean position between the contact points,

$$\mathbf{o}_m = \frac{1}{n^m}\sum_{j=1}^{n^m} \mathbf{p}^m_j \qquad \mathbf{o}_s = \frac{1}{n^s}\sum_{l=1}^{n^s} \mathbf{p}^s_l \ , \tag{35}$$

where $\mathbf{p}^m_j$ and $\mathbf{p}^s_l$ are the interaction/contact points on the master and slave sides respectively. During task execution, motion along the x-axis are negligible. The scaling factors

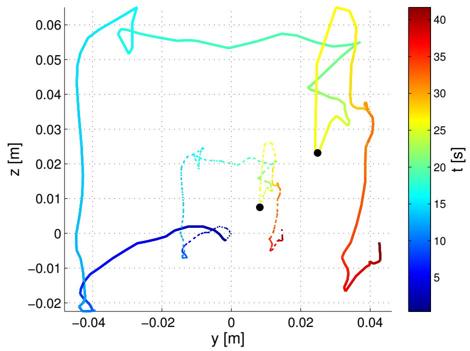

Fig. 8. Trajectories of master (dotted) and slave (solid) virtual objects centers defined in Eq. (35). The color bar on the right indicates the elapsed time throughout the task. The two black dots highlight the sudden change in the trajectory at $t = 24.64$ s due to the contact with the punctured board.

$\alpha = 3$ and $\beta = 1$ were used to match master and slave workspaces, see Eq. (14). A color bar has been added on the right of the figure to provide the reader with the time information about the position of the virtual objects throughout the carried out task. At $t = 24.64$ s a collision between the peg and the board occurred as it is reported in Fig. 8 by the sudden change in direction of the trajectory along the z-axis.

Fig. 9 reports the forces displayed on the master side through the two haptic devices during the task execution. The scaling factor η introduced in Eq. (6) was set to one. On the left side of the figure, we refer to the device connected to the user's thumb, while on the right side we refer to the other haptic interface connected to the user's index finger. With dotted red lines we show the forces computed through the backward mapping. The forces that are limited by the passivity layer to prevent instability are drawn in blue. These forces are those actually provided to the users through the haptic interfaces while performing the task. Starting from the top (Figs. 9a and 9b), the robotic hand does not apply significant forces along the x-axis, in line with the proposed task. Figs. 9c and 9d show the forces that render the grasp tightness to the user. In fact, the y-axis in this task configuration contains internal forces. The oscillations before $t = 10$ s, are mostly due to the adjustments needed during the grasping action and to some contact between the peg and the borders of the hole, which the parallelepiped was raised from. In Figs. 9e and 9f the forces due to the gravity action along the z-axis are reported. Such forces basically are an estimation of the weight of the peg (254 g) obtained by the torque sensors placed in the robotic hand joints. The peak at $t = 24.64$ s is due to the contact between the peg and the board occurred before inserting correctly the object inside the $hole_2$ as shown also in Fig. 8. Right afterwards, when the peg is raised again only the gravity force acts along the z-axis until the object is released.

In Fig. 10 the sum of the magnitude of internal and external forces rendered on the master side is shown using a solid blue line and a dash-dotted red line respectively. When the object is not grasped, both forces are nearly zero. During the grasping action there is an increase of the internal force due to the squeezing action commanded by the user. Then forces become quite stationary until $t = 24.64$ s, when due to the contact of the peg with the external and stiff environment the

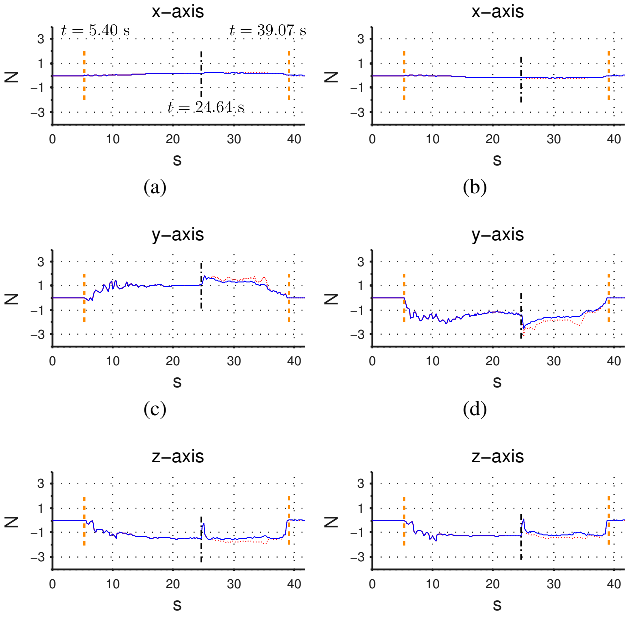

(a) (b)

(c) (d)

(e) (f)

Fig. 9. Forces displayed by the two haptic devices during the task execution. On the abscissa the time is shown. Plots on the left are referred to forces provided to the user's thumb through the haptic interface end-effector, while on the right, to the forces rendered on the index finger. Dotted red lines represent the force that guarantee the complete transparency of the teleoperation system. Blue lines represent forces actually provided to the user. Original values are properly limited by the passivity layer to preserve stability. At $t = 5.40\,\mathrm{s}$ and $t = 39.07\,\mathrm{s}$ (dashed orange line) the contact between the robotic hand and the object occurs and is interrupted respectively. At $t = 24.64\,\mathrm{s}$ (dash-dot black line) the contact between the peg and the support base occurs.

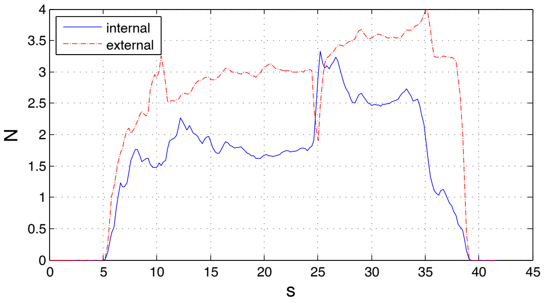

Fig. 10. Magnitudes of the internal and external forces acting on the slave side. The total amount of forces is measured through the torque sensors placed at the robotic fingers joints.

external force is compensated by the interaction force and gets lower. At the same time, the user, who perceives the action of an external and unexpected force, tends to squeeze the object (internal forces) more to increase the grasp stability. The user reaction was registered even if the motion of the slave contact points generating the external and internal forces on the slave side are computed separately by the forward mapping.

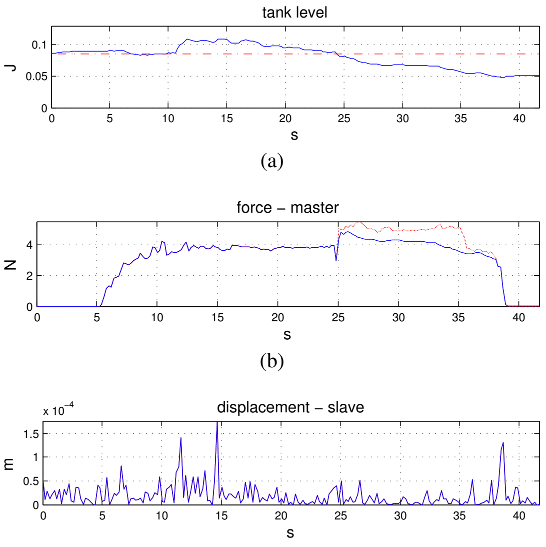

(a)

(b)

(c)

Fig. 11. Two-layer passivity approach. (a) The tank level is reported and the dashed-dotted red line shows the desired tank level H_d. (b) The dotted red line represents the sum of the magnitudes of the original forces computed on the slave side, while the blue line indicates the sum of the magnitudes of the forces actually provided through the haptic interfaces and limited due to the passivity control layer. (c) The dotted red line shows the sum of the displacements of each contact point at the slave side per time step, while the blue line indicates the sum of the displacements of each contact point limited with respect to the available energy present in the tank. In this specific case no cutting has been needed on the slave side to ensure the stability of the system, so the two lines are overlapped. On the abscissa the elapsed time is always reported.

Fig. 11 deals with the two-layer passivity approach. A preliminary tuning phase was necessary to properly set the parameters of the proposed passivity approach according to the teleoperation system at hand, i.e., $H_d = 0.085\,\mathrm{J}$, $\nu = 300\,\mathrm{N\,s/m\,J}$, $\Delta F_{rb}^{max} = 20\,\mathrm{N}$, $\Delta F_{def}^{max} = 20\,\mathrm{N}$, $\Delta p^{max} = 0.015\,\mathrm{m}$. Fig. 11a shows a decrease in the tank level when $t > 24.64\,\mathrm{s}$. This is related to the contact between the peg and the support base, a mostly dissipative action which requires an unexpected and high demand of energy. Then the available energy gets lower than H_d (dashed-dotted red line in the figure) and the passivity layer limits the displayed force at master side to ensure the stability of the whole system. We do not report in the plot the initial phase during which the tank is filled to the desired level H_d ("Energy Extraction" phase in [6]). A modulated viscous damper is used to oppose the user's movement and transfer energy from the user to the tank. The difference between original and limited forces can be appreciated in Fig. 11b in terms of the sum of the force magnitudes provided to the user, or in Fig. 9 as the forces rendered per haptic device and axis of application. However, in this specific case the implemented two-layer approach does not limit the displacement of the contact points on the slave side (see the Fig. 11c). This means that there is sufficient energy in the tank to allow a transparent motion of the robotic hand/arm system. For the same amount of energy in the tank ($H(k)$) the cutting action on the master and slave sides can be different, since it depends on their current energy request, and on the a priori chosen parameters Δp^{max}, ΔF_{rb}^{max}, ΔF_{def}^{max}.

Remark 6: In the proposed bilateral telemanipulation framework forces/positions of interaction points on master side and contact points on slave side cannot be compared one to one. The aim of this work is to consider different number of contact and interaction points. For this reason, we considered an aggregated information represented by the virtual object centers (Fig. 8) to prove tracking capability of the system, while to evaluate force rendering we reported the single forces on the master side and internal and external force magnitudes

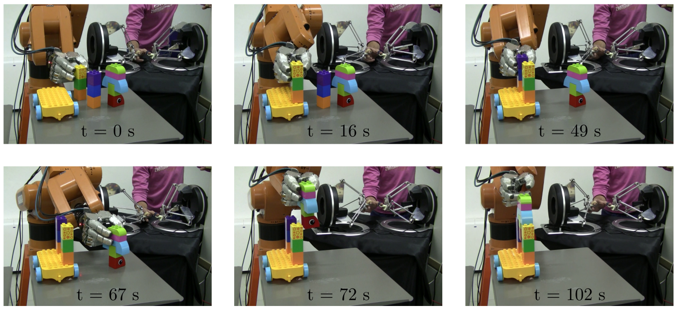

Fig. 12. Time-lapse sequence of an assembly of LEGO bricks. The task consisted in picking three bricks from a table and assemble them in a required configuration. On the bottom of each image the relative elapsed time t is depicted.

(Fig. 10) as aggregated information of the forces on the slave side.

B. Assembly of LEGO bricks

As additional experiment, we performed a manipulation task consisting in assembling LEGO bricks contained in the YCB object and model set [39]. LEGO bricks are made with extremely tight tolerances and assembling them with a telemanipulation system is a challenge. The operator was asked to pick three different bricks placed on a table at the slave site and assemble them in a specific configuration. The final result shows how the proposed telemanipulation system can guarantee fine manipulation skills and a fine control of exerted forces to accomplish such a task. Six frames of the task execution are shown in Fig. 12 with the relative elapsed time.

V. CONCLUSION

We presented a telemanipulation framework that can deal with kinematic asymmetries between master and slave structures. The force feedback has been computed by imposing the same wrench, estimated on the real grasped object, on a virtual object defined at the master side. This solution focuses on the effects on the manipulated object and allows to abstract from the device kinematics and consider multi-contact scenarios. The proposed approach has been validated with an experimental setup where the master is represented by two haptic interfaces, while the slave is a robotic hand/arm system. The bilateral teleoperation framework proposed in the paper can be extended to cooperative robot formations and wearable haptic master systems, as that proposed in [40]. In particular, multi-contact rendering with wearable haptic interfaces, can overcome the workspace problems of the classical single-contact haptic devices, but a tracking system would be required to identify the position of each contact point on the master side.

As a natural development of this work, we are planning to substitute the grounded haptic interfaces exploited in the proposed setup with lighter devices that can be directly worn on the user's fingertips. We are also testing different models of robotic hands at the slave side, with particular emphasis on non-anthropomorphic structures. Finally, we will extend the framework to robots cooperatively grasping an object.

REFERENCES

[1] P. F. Hokayem and M. W. Spong, "Bilateral teleoperation: An historical survey," *Automatica*, vol. 42, no. 12, pp. 2035–2057, 2006.

[2] P. Arcara and C. Melchiorri, "Control schemes for teleoperation with time delay: A comparative study," *Robotics and Autonomous Systems*, vol. 38, no. 1, pp. 49–64, 2002.

[3] K. Hashtrudi-Zaad and S. E. Salcudean, "Analysis of control architectures for teleoperation systems with impedance/admittance master and slave manipulators," *The International Journal of Robotics Research*, vol. 20, no. 6, pp. 419–445, 2001.

[4] D. Lee and K. Huang, "Passive-set-position-modulation framework for interactive robotic systems," *Robotics, IEEE Transactions on*, vol. 26, no. 2, pp. 354–369, 2010.

[5] R. Cortesão, J. Park, and O. Khatib, "Real-time adaptive control for haptic telemanipulation with kalman active observers," *Robotics, IEEE Transactions on*, vol. 22, no. 5, pp. 987–999, 2006.

[6] M. Franken, S. Stramigioli, S. Misra, C. Secchi, and A. Macchelli, "Bilateral telemanipulation with time delays: A two-layer approach combining passivity and transparency," *Robotics, IEEE Transactions on*, vol. 27, no. 4, pp. 741–756, 2011.

[7] J.-P. Kim and J. Ryu, "Robustly stable haptic interaction control using an energy-bounding algorithm," *The International Journal of Robotics Research*, vol. 29, no. 6, pp. 666–679, 2010.

[8] F. Barbagli, K. Salisbury, and D. Prattichizzo, "Dynamic local models for stable multi-contact haptic interaction with deformable objects," in *Haptic Interfaces for Virtual Environment and Teleoperator Systems, Proc. 11th Symp. on*, pp. 109–116, 2003.

[9] A. Franchi, C. Secchi, H. I. Son, H. Bulthoff, and P. Giordano, "Bilateral teleoperation of groups of mobile robots with time-varying topology," *Robotics, IEEE Transactions on*, vol. 28, no. 5, pp. 1019–1033, 2012.

[10] E. Rodrìguez-Seda, J. Troy, C. Erignac, P. Murray, D. Stipanovic, and M. Spong, "Bilateral teleoperation of multiple mobile agents: Coordinated motion and collision avoidance," *Control Systems Technology, IEEE Transactions on*, vol. 18, no. 4, pp. 984–992, 2010.

[11] R. Mohajerpoor, I. Sharifi, H. A. Talebi, and S. M. Rezaei, "Adaptive bilateral teleoperation of an unknown object handled by multiple robots under unknown communication delay," in *Advanced Intelligent Mechatronics (AIM), 2013 IEEE/ASME International Conference on*, pp. 1158–1163, IEEE, 2013.

[12] F. Barbagli and K. Salisbury, "The effect of sensor/actuator asymmetries in haptic interfaces," in *Haptic Interfaces for Virtual Environment and Teleoperator Systems, 2003. HAPTICS 2003. Proceedings. 11th Symposium on*, pp. 140–147, IEEE, 2003.

[13] L. N. Verner and A. M. Okamura, "Sensor/actuator asymmetries in telemanipulators: Implications of partial force feedback," in *Haptic Interfaces for Virtual Environment and Teleoperator Systems, 2006 14th Symposium on*, pp. 309–314, IEEE, 2006.

[14] P. Malysz and S. Sirouspour, "Trilateral teleoperation control of kinematically redundant robotic manipulators," *The International Journal of Robotics Research*, vol. 30, no. 13, pp. 1643–1664, 2011.

[15] P. Malysz and S. Sirouspour, "A kinematic control framework for single-slave asymmetric teleoperation systems," *Robotics, IEEE Transactions on*, vol. 27, no. 5, pp. 901–917, 2011.

[16] R. Kubo, T. Shimono, and K. Ohnishi, "Flexible controller design of bilateral grasping systems based on a multilateral control scheme," *Industrial Electronics, IEEE Transactions on*, vol. 56, no. 1, pp. 62–68, 2009.

[17] A. Peer, S. Einenkel, and M. Buss, "Multi-fingered telemanipulation - mapping of a human hand to a three finger gripper," in *Robot and Human Interactive Communication, 2008. RO-MAN 2008. The 17th IEEE International Symposium on*, pp. 465–470, August 2008.

[18] J. L. Graham, S. G. Manuel, M. S. Johannes, and R. S. Armiger, "Development of a multi-modal haptic feedback system for dexterous robotic telemanipulation," in *Systems, Man, and Cybernetics (SMC), 2011 IEEE International Conference on*, pp. 3548–3553, IEEE, 2011.

[19] S. Sirouspour, "Modeling and control of cooperative teleoperation systems," *Robotics, IEEE Transactions on*, vol. 21, no. 6, pp. 1220–1225, 2005.

[20] D. Lee and M. W. Spong, "Bilateral teleoperation of multiple cooperative robots over delayed communication networks: theory," in *Robotics and Automation, 2005. ICRA 2005. Proceedings of the 2005 IEEE International Conference on*, pp. 360–365, IEEE, 2005.

[21] G. Gioioso, A. Franchi, G. Salvietti, S. Scheggi, and D. Prattichizzo, "The flying hand: A formation of uavs for cooperative aerial telemanipulation," in *Proc. IEEE Int. Conf. on Robotics and Automation*, pp. 4335–4341, 2014.

[22] G. Gioioso, G. Salvietti, M. Malvezzi, and D. Prattichizzo, “An object-based approach to map human hand synergies onto robotic hands with dissimilar kinematics,” in *Robotics: Science and Systems VIII*, Sidney, Australia: The MIT Press, July 2012.

[23] G. Gioioso, G. Salvietti, M. Malvezzi, and D. Prattichizzo, “Mapping synergies from human to robotic hands with dissimilar kinematics: an approach in the object domain,” *IEEE Trans. on Robotics*, vol. 29, pp. 825–837, August 2013.

[24] G. Salvietti, L. Meli, G. Gioioso, M. Malvezzi, and D. Prattichizzo, “Object-based bilateral telemanipulation between dissimilar kinematic structures,” in *Proc. IEEE/RSJ Int. Conf. Intelligent Robots and Systems*, (Tokyo, Japan), pp. 5451–5456, 2013.

[25] W. Griffin, R. Findley, M. Turner, and M. Cutkosky, “Calibration and mapping of a human hand for dexterous telemanipulation,” in *ASME IMECE 2000 Symposium on Haptic Interfaces for Virtual Environments and Teleoperator Systems*, pp. 1–8, 2000.

[26] G. Salvietti, M. Malvezzi, G. Gioioso, and D. Prattichizzo, “On the use of homogeneous transformations to map human hand movements onto robotic hands,” in *Proc. IEEE Int. Conf. on Robotics and Automation*, (Hong Kong, China), 2014.

[27] K. Shoemake and T. Duff, “Matrix animation and polar decomposition,” in *Proceedings of the conference on Graphics interface*, vol. 92, pp. 258–264, Citeseer, 1992.

[28] R. Goldman, *Recovering the Data from the Transformation Matrix*, vol. VII-2 of *GEMS*. Academic Press, 1991.

[29] N. J. Higham and R. S. Schreiber, “Fast polar decomposition of an arbitrary matrix,” *SIAM Journal on Scientific and Statistical Computing*, vol. 11, no. 4, pp. 648–655, 1990.

[30] D. Prattichizzo and J. Trinkle, “Grasping,” in *Handbook on Robotics* (B. Siciliano and O. Kathib, eds.), pp. 671–700, Springer, 2008.

[31] R. Murray, Z. Li, and S. Sastry, *A mathematical introduction to robotic manipulation*. CRC, 1994.

[32] A. Bicchi, “On the closure properties of robotic grasping,” *The Int. J. of Robotics Research*, vol. 14, no. 4, pp. 319–334, 1995.

[33] G. Baud-Bovy, D. Prattichizzo, and N. Brogi, “Does torque minimization yield a stable human grasp?,” *Multi-point Interaction with Real and Virtual Objects*, pp. 21–40, 2005.

[34] D. Prattichizzo, M. Malvezzi, M. Gabiccini, and A. Bicchi, “On motion and force controllability of precision grasps with hands actuated by soft synergies,” *IEEE Transactions on Robotics*, vol. 29, no. 6, pp. 1440–1456, 2013.

[35] N. Hogan, “Controlling impedance at the man/machine interface,” in *Proc. IEEE International Conference on Robotics and Automation (ICRA)*, pp. 1626–1631, 1989.

[36] A. J. van der Schaft, *L2-gain and passivity techniques in nonlinear control*. Springer Verlag, 2000.

[37] G. Niemeyer and J. J. E. Slotine, “Telemanipulation with time delays,” *The International Journal of Robotics Research*, vol. 23, no. 9, pp. 873–890, 2004.

[38] J. Ryu, D. Kwon, and B. Hannaford, “Stable teleoperation with time-domain passivity control,” *IEEE Transactions on Robotics and Automation*, vol. 20, no. 2, pp. 365–373, 2004.

[39] B. Calli, A. Walsman, A. Singh, S. Srinivasa, P. Abbeel, and A. M. Dollar, “Benchmarking in manipulation research: The ycb object and model set and benchmarking protocols,” *arXiv preprint arXiv:1502.03143*, 2015.

[40] Z. Ma and P. Ben-Tzvi, “Rml glove - an exoskeleton glove mechanism with haptics feedback,” *Mechatronics, IEEE/ASME Transactions on*, vol. 20, pp. 641–652, April 2015.

Gionata Salvietti (M’12) received the M.S. degree in Robotics and Automation and the Ph.D. degree in Information Engineering from the University of Siena, Siena, Italy, in 2009 and 2012, respectively. He was a post-doc researcher with the Istituto Italiano di Tecnologia from 2012 to 2015. He is currently Assistant Professor at Department of Information Engineering and Mathematics, University of Siena and Research Affiliate at Dept. of Advanced Robotics at Istituto Italiano di Tecnologia. His research interests are telemanipulation, robotic and human grasping, assistive devices, and haptics.

Leonardo Meli (S’13) received the M.S. degree in Computer and Automation Engineering and the Ph.D. degree in Information Engineering from the University of Siena, Siena, Italy, in 2012 and 2016, respectively. He was an exchange student at the Karlstad University, Sweden in 2010. He spent the last 4 months of 2015 visiting the BioInstrumentation Laboratory at the Massachusetts Institute of Technology, Cambridge, Ma, USA. His research interests include robotics and haptics focusing on cutaneous force feedback techniques, teleoperation systems for medical applications, and grasping.

Guido Gioioso received the “Laurea Specialistica” (con Lode) in Information Engineering from the Univesity of Siena in 2011. He is currently a Ph.D. student at the Department of Information Engineering and Mathematics of the University of Siena and at the Department of Advanced Robotics, Istituto Italiano di Tecnologia. His research interests are robotic and human grasping, haptics, teleoperation and mobile robots.

Monica Malvezzi (M’12) is Assistant Professor of Mechanics and Mechanism Theory at the Department of Information Engineering and Mathematics of the University of Siena. She received the Laurea degree in Mechanical Engineering from the University of Florence in 1999 and the Ph.D. degree in Applied Mechanics from the University of Bologna in 2003. Since 2015 she is Visiting Scientist at the Department of Advanced Robotics, Istituto Italiano di Tecnologia. Her main research interests are in control of mechanical systems, robotics, vehicle localization, multibody dynamics, haptics, grasping and dexterous manipulation.

Domenico Prattichizzo (F’16) received the M.S. degree in Electronics Engineering and the Ph.D. degree in Robotics and Automation from the University of Pisa in 1991 and 1995, respectively. Since 2015, Fellow IEEE. Since 2015 Full Professor of Robotics at the University of Siena. Since 2009 Scientific Consultant at Istituto Italiano di Tecnologia, Genova Italy. From 2007 to 2014, Associate Editor in Chief of the IEEE Trans. on Haptics. From 2003 to 2007, Associate Editor of the IEEE Trans. on Robotics and IEEE Trans. on Control Systems Technologies. Research interests are in haptics, grasping and medical robotics.